Mesh Resolution Influence on the SAR Distribution in Human Head Model

Arkadiusz Miaskowski, Bartosz Sawicki, Andrzej Krawczyk

Abstract — **The paper presents the numerical calculation of SAR (*ang. Specific Absorption Rate*) distribution in realistic human head model resolved into an equidistant mesh of spacing (from 4mm up to 17mm). Authors utilized the "visible man" model derived from a project under the direction of the National Library of Medicine to investigate mesh resolution influence on the SAR distribution. The calculations are based on commercially available FDTD (*Finite Difference Time Domain*) package from Empire^{TM} by IMST.**

I. Introduction

The increasing use of radio-based portable communication devices has created public concern about their safety despite reports finding no substantive scientific evidence of a long-term public health hazard [1]. The proximity of these devices to the body during their operation leads to highly no uniform exposure and so it is inappropriate to specify limits based on electric and magnetic fields and power density [2]. Limits are therefore specified in terms of the actual rate of radio frequency energy absorption. The SAR is calculated from the electric field strength $\boldsymbol{E}$ inside the human body, the conductivity σ and the mass density ρ of the biological tissue:

$$SAR = \sigma \frac{\boldsymbol{E}^2}{\rho} \tag{1}$$

and is averaged out to mass of 1g or 10 g of tissue in the shape of cube.

Government agencies have announced plans to regulate portable radio transmitting devices based on these limits and this has led to a need for effective means of SAR or through electromagnetic methods. Presently direct measurement method are preferred due to the ability to the accuracy of the system and the difficulties of modeling the intricate details of individual handsets.

There have been a number of theoretical models used to obtain inducted field and SAR distribution in humans exposed to radiofrequency fields. These models have varied form simple spherical forms consisting of a single tissue used in early history of bioelectromagnetics research to realistic true – form multi – tissue replicas of humans in use today [3]. With today's computers and workstations it is possible to obtain high resolution of SAR distribution in exposed biological models represented by a mesh. These models (the meshes) provided significant insight into how RF (*Radio Frequency*) energy is absorbed in exposed subjects. That is why authors decided to investigate how SAR distribution depends on mesh resolution of model.

II. Finite-Difference Time-Domain

Authors used FDTD technique to investigate mesh resolution influence on the SAR distribution. There are several advantages of this method over frequency-domain techniques such as the finite-element method FEM and boundary integral methods. First, the method is a direct solution of Maxwell's time-domain equations. Consequently, it is a complete full-wave solution that contains no approximations that would prevent a correct solution from being reached. FEM and integral methods can be plagued by spurious nonphysical solutions. Second, the method is extremely general in the materials and geometries it can analyze. Structures that contain inhomogeneous, lossy, or even anisotropic material properties can be easily handled. Last and most important, the memory requirements of the FDTD are significantly less than those of other methods, which allows for efficient analysis of electrically large scatterers. The only disadvantage of FDTD method is problem with smooth shape of objects, which is hard to describe with structured mesh.

The FDTD method derives its name from a direct finite-difference approximation to Maxwell's time-dependent curl equations,

$$\frac{\partial \boldsymbol{H}}{\partial t} = -\frac{1}{\mu}\nabla \times \boldsymbol{E}, \quad \frac{\partial \boldsymbol{E}}{\partial t} = -\frac{1}{\varepsilon}\nabla \times \boldsymbol{H} - \frac{\sigma}{\varepsilon}\boldsymbol{E} \tag{2}$$

where boldface is used to represent a vector quantity.

In a 3D rectangular coordinate system these equations can be expanded into an equivalent system of six coupled scalar equations for all electric and magnetic field components,

$$\frac{\partial \boldsymbol{H}_x}{\partial t} = \frac{1}{\mu}\left(\frac{\partial \boldsymbol{E}_z}{\partial y} - \frac{\partial \boldsymbol{E}_y}{\partial z}\right), \quad \frac{\partial \boldsymbol{E}_x}{\partial t} = \frac{1}{\varepsilon}\left(\frac{\partial \boldsymbol{E}_z}{\partial y} - \frac{\partial \boldsymbol{E}_y}{\partial z} - \sigma \boldsymbol{E}_x\right) \tag{3}$$

$$\frac{\partial \boldsymbol{H}_y}{\partial t} = \frac{1}{\mu}\left(\frac{\partial \boldsymbol{E}_x}{\partial z} - \frac{\partial \boldsymbol{E}_z}{\partial x}\right), \quad \frac{\partial \boldsymbol{E}_y}{\partial t} = \frac{1}{\varepsilon}\left(\frac{\partial \boldsymbol{E}_x}{\partial z} - \frac{\partial \boldsymbol{E}_z}{\partial x} - \sigma \boldsymbol{E}_y\right) \tag{4}$$

$$\frac{\partial \boldsymbol{H}_z}{\partial t} = \frac{1}{\mu}\left(\frac{\partial \boldsymbol{E}_y}{\partial x} - \frac{\partial \boldsymbol{E}_x}{\partial y}\right), \quad \frac{\partial \boldsymbol{E}_z}{\partial t} = \frac{1}{\varepsilon}\left(\frac{\partial \boldsymbol{E}_y}{\partial x} - \frac{\partial \boldsymbol{E}_x}{\partial y} - \sigma \boldsymbol{E}_z\right) \tag{5}$$

A. Miaskowski and A. Krawczyk are with the Electrotechnical Institute in Warsaw, Pozaryskiego 28, 04-703 Warszawa, Poland, e-mail: *a.miaskowski@iel.waw.pl*

B. Sawicki is with the Institute of Theory of Electrical Engineering, Measurement and Information Systems, Warsaw University of Technology, ul. Koszykowa 75, 00-662 Warszawa, Poland, e-mail: *sawickib@iem.pw.edu.pl*

Yee's basic scheme is to use a series of finite difference approximations to transform Eqs. (3)–(4) into a system of six algebraic equations. These equations can then be solved with a simple leap-frog algorithm. As an illustration we provide here the FDTD approximation for the $\boldsymbol{E}_x$ field component,

$$E_x\big|_{i,j,k}^{n+1} = \frac{1-\sigma_{i,j,k}\Delta t/2\varepsilon_{i,j,k}}{1+\sigma_{i,j,k}\Delta t/2\varepsilon_{i,j,k}} + \frac{\Delta t/2\varepsilon_{i,j,k}}{1+\sigma_{i,j,k}\Delta t/2\varepsilon_{i,j,k}}\frac{1}{\Delta y}\left(H_z\big|_{i,j+1/2,k}^{n+1/2} - H_z\big|_{i,j-1/2,k}^{n+1/2}\right) - \frac{\Delta t/2\varepsilon_{i,j,k}}{1+\sigma_{i,j,k}\Delta t/2\varepsilon_{i,j,k}}\frac{1}{\Delta z}\left(H_y\big|_{i,j,k+1/2}^{n+1/2} - H_z\big|_{i,j,k-1/2}^{n+1/2}\right) \quad (6)$$

where *i*, *j*, and *k* indices represent the *x*, *y*, and *z* spatial location, respectively; n indicates the current time index; Δy and Δz represent the y and the z spatial increments, respectively; ε, σ, and μ represent the permittivity, electric conductivity, and magnetic permeability, respectively; and Δt is the time step. The unknown field distribution over a finite space is calculated by application of the six FDTD equations to a volumetrically sampled grid of cells called Yee cells. Each edge of a Yee cell may be assigned independent electrical properties, which allows one to model complex objects that can consist of lossy, inhomogenous, or anisotropic materials.

Figure 1 illustrates how the field components are assigned to a unit Yee cell. We should note that the ½ time-step values, used in the $n+½$ terms in Eq. (6), denote the sequential order of the FDTD computations. For instance, in Eq. (6) the magnetic field, at the $n+½$ time step, was determined with the electric field value at the previous *n*th time step. In turn this magnetic field value is now being used to determine the electric field at the current time value, $n+1$. This leap-frog process is continued until the FDTD computations are complete. This algorithm is generally referred to as the Yee, or time-marching, algorithm.

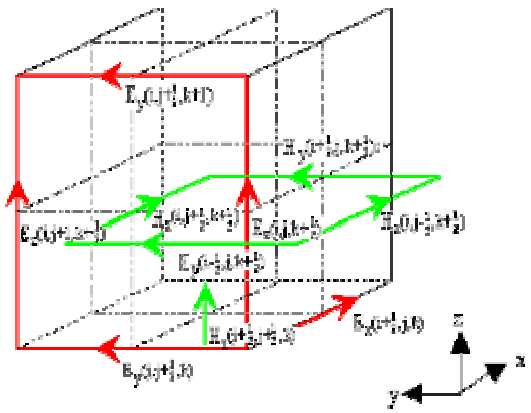

Fig.1. Positions of electric and magnetic field components on Yee cell in rectangular coordinates.

III. HUMEN HEAD MODEL

The aim of the paper was to show the adequacy of human head mesh (size) resolution with SAR distribution. Human head model is based on set of slices from Visible Human Project [4]. Using data from slices authors produced mesh resolution 1x1x1mm but such a resolution exceed authors computer hardware abilities. That is why research covered mesh resolutions from 4x4x4 mm up to 17x17x17 mm.

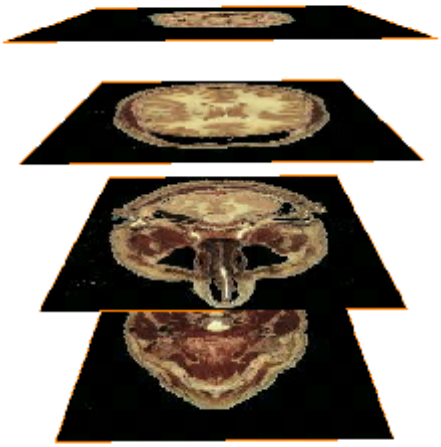

Fig 2. Creating a realistic model: few sample cross – section of the head from Visible Human database [4].

Each of the four identified head tissues (skin, skull, brain, eye tissue) in the slices, was coded with numbers referring to its unique dielectric properties for 900 MHz , resulting in three dimensional FDTD mesh from 4x4x4 mm up to 17x17x17 mm size. The density and the proper dielectric properties of tissues are shown in Table I.

TABLE I. DIELECTRIC PROPERTIES OF TISSUES FOR 900 MHZ [5]

Tissue	ε_r	σ **[S/m]**	ρ **[g/cm^3]**
Skin	46.1	0.84	1.04
Skull	16.62	0.24	1.85
Brain	45.8	0.76	1.03
Eye tissue (Sclera)	55.27	1.16	1.05

The exemplary construction of the head models of 4x4x4 mm and 10x10x10 mm mesh size are shown in Figure 3 and Figure 4.

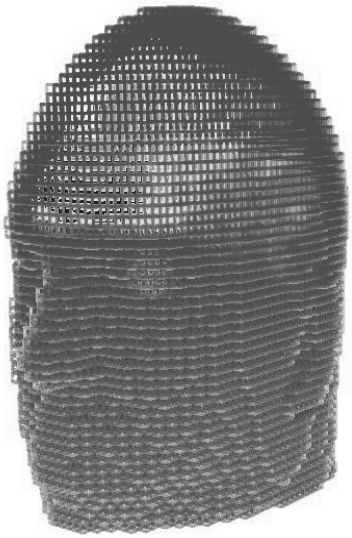

Fig 3. Human head model (4x4x4 mm mesh size, 114492 voxels)

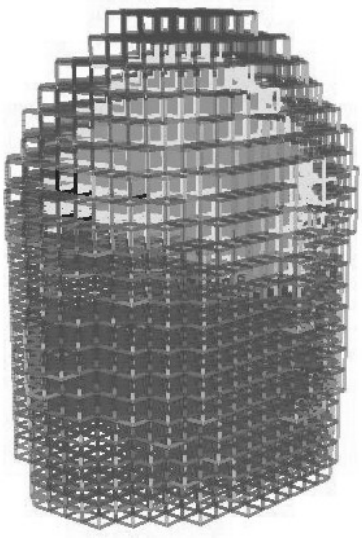

Fig 4. Human head model (10x10x10 mm mesh size, 5544 voxels)

IV. Human Head Exposed To Plane Wave

In order to investigate the adequacy of human head mesh resolution with SAR distribution authors used from 4x4x4 mm up to 17x17x17 mm meshed models. These models consist of four different tissues, including a layer of skin, a layer of skull, a layer of brain and a layer of eyes tissues. Moreover, the dielectric properties for each of the layers have been added. The SAR was calculated over *x-z* plane cross section of the model exposed to 900 MHz plane wave with the wave incident vector parallel to *x* axis and E-field vector parallel to *z* axis. The SAR also was averaged out to 10 grams of tissue centered about the corner of each voxel.

The exemplary plots of the calculated SAR averaged over 10grams of tissue for 4x4x4mm and 10x10x10mm mesh size are shown in Figure 5 and Figure 6. Moreover, values of maximum SAR, averaged SAR and scattered power of each of the nine mesh resolutions are collected in Table I. We can also see the results on the charts (Fig.7,8,9)

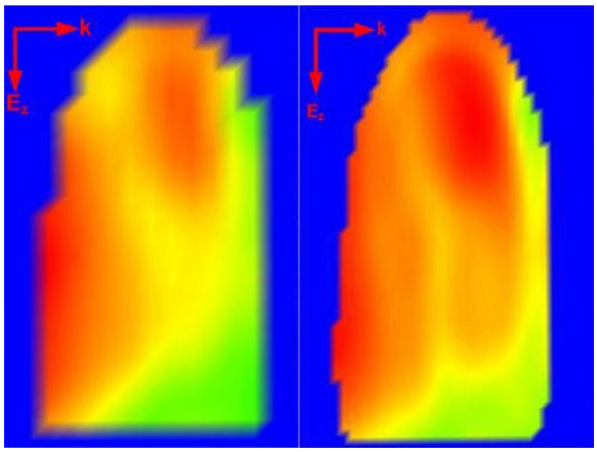

Fig 5. SAR distribution in x-z plane for 10x10x10 and 4x4x4 mm mesh size

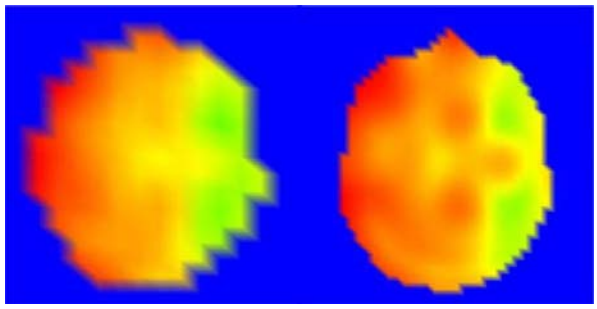

Fig 6. SAR distribution in x-y plane for 10x10x10 and 4x4x4 mm mesh size

Table II. SAR For Different Mesh Resolutions

Mesh size [mm]	Max. SAR [mW/g]	Avg. SAR_{10g} [mW/g]	Volume of model [mm^3]
17x17x17	21,9	5,778	9079224
13x13x13	18,38	4,002	8304660
10x10x10	10,02	4,148	8280000
9x9x9	14,6	3,812	7922772
8x8x8	13,12	3,42	7839744
7x7x7	12,96	3,946	7640325
6x6x6	10,7	3,256	7354368
5x5x5	11,32	3,212	7267500
4x4x4	10,66	3,12	7074816

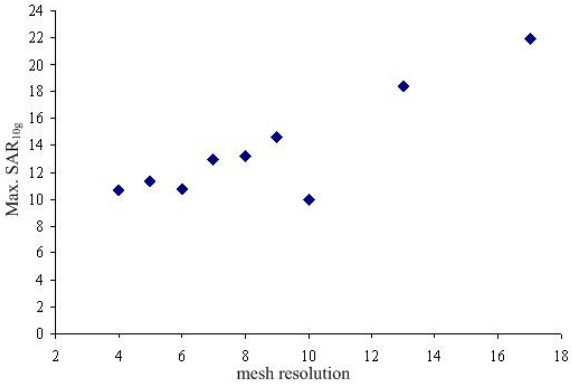

Fig 7. Maximum SAR_{10g} dependence on mesh resolution

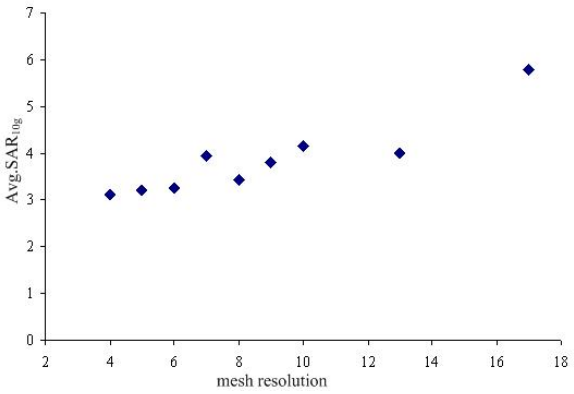

Fig 8. Average SAR_{10g} dependence on mesh resolution

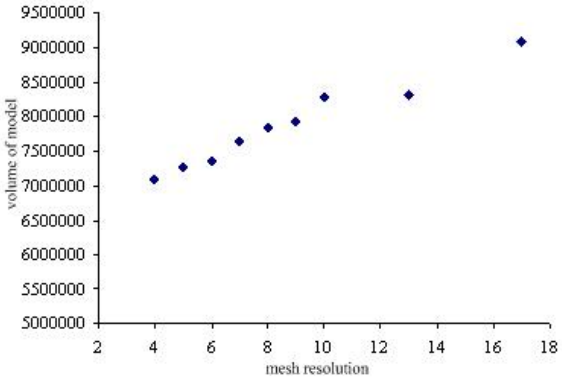

Fig 9. Mesh resolution dependence on volume of head model

It is obvious that resolution of mesh increase resolution of results but more interesting remark is that higher resolution showed some small fluctuations of SAR inside human head, see Fig. 5,6. Using charts presented on Fig. 7,8, authors conclude that size of mesh element can significantly change results. Although general trend is that bigger voxels gives higher SAR, but we have to remember that those results are with bigger discretization errors. Unfortunately discretization errors of non-technical objects with real, smooth shapes are a little bit unpredictable. We are sure, that increasing resolution should give better results, but this is only global rule - like in optimization process local minimals can appear.

V. CONCLUSIONS

The finite-difference time-domain (FDTD) method was presented as an efficient means of performing three-dimensional (3D) analysis of Specific Absorption Rate (SAR). Authors used Visible Human Project developed by U.S. National Library of Medicine in order to construct a human head model and investigate mesh resolution influence on the SAR distribution in the human head model and showed that discretization of real medicine objects such as human head is always a hard problem. Authors showed that resolution of mesh has significant influence on the SAR distribution inside human head calculated using FDTD method. More dense meshes gives more accurate SAR distribution, but maximal and averaged values can change unexpectedly.

REFERENCES

[1] International Commission Non-Ionizing Radiation Protection, "Health issues to the use of hand-held radiotelephones and base transmitters", Health Phys., vol. 70, no. 4, pp. 587-593, Apr.1996.

[2] N. Kuster, Q. Balzano, "Energy absorption mechanism by biological bodies in the near field of dipole antennas above 300 MHz", IEEE Trans. Veh. Technol., vol. 41, pp. 17-23, Feb. 1992.

[3] A. Guy, "Dosimetry of Radiofrequency Electromagnetic Fields: Examples of Results Using Numerical Methods", Department of Bioengineering, University of Washington.

[4] http://www.nlm.nih.gov/research/visible/visible_human.html.

[5] Gabriel C, "Compilation of the Dielectric Properties of Body Tissues at RF and Microwave Frequencies", Brooks Air Force Bse, report no AL./OE-TR-1996-0037,1996.